Identification of the endocytic sorting signal recognized by the Art1-Rsp5 ubiquitin ligase complex

Evan L. Guiney[†], Till Klecker[†], and Scott D. Emr*

Weill Institute for Cell and Molecular Biology and Department of Molecular Biology and Genetics, Cornell University, Ithaca, NY 14853

ABSTRACT Targeted endocytosis of plasma membrane (PM) proteins allows cells to adjust their complement of membrane proteins to changing extracellular conditions. For a wide variety of PM proteins, initiation of endocytosis is triggered by ubiquitination. In yeast, arrestin-related trafficking adaptors (ARTs) enable a single ubiquitin ligase, Rsp5, to specifically and selectively target a wide range of PM proteins for ubiquitination and endocytosis. However, the mechanisms that allow ARTs to specifically recognize their appropriate substrates are unknown. We present the molecular features in the methionine permease Mup1 that are required for Art1-Rsp5–mediated ubiquitination and endocytosis. A combination of genetics, fluorescence microscopy, and biochemistry reveals three critical features that comprise an ART sorting signal in the Mup1 N-terminal cytosolic tail: 1) an extended acidic patch, 2) in close proximity to the first Mup1 transmembrane domain, and 3) close to the ubiquitinated lysines. We show that a functionally similar ART sorting signal is also required for the endocytosis of a second Art1-dependent cargo, Can1, suggesting a common mechanism for recognition of Art1 substrates. We isolate two separate suppressor mutations in the Art1 C-terminal domain that allele-specifically restore endocytosis of two Mup1 acidic patch mutants, consistent with an interaction between the Art1 C-terminus and the Mup1 acidic patch. We propose that this interaction is required for recruitment of the Art1-Rsp5 ubiquitination complex.

INTRODUCTION

The plasma membrane (PM) is the outermost cellular membrane, physically separating intracellular and extracellular space. It contains an elaborate protein network that mediates and controls the exchange between cells and their extracellular space, thus governing virtually every aspect of cellular physiology. Hence cells have to constantly control the PM protein composition in response to extracellular signals and stress. Remodeling of the PM protein composition requires biosynthesis of new proteins, as well as removal of existing proteins from the PM. Protein transport to the cell surface is mediated by sorting of these proteins into vesicles at the Golgi or recycling endosomes (Feyder *et al.*, 2015). By contrast, ubiquitin-mediated endocytosis provides a mechanism to selectively remove proteins destined for removal from the PM (MacGurn *et al.*, 2012).

Ubiquitination of PM proteins initiates their endocytosis and subsequent transfer to lysosomes for degradation (Piper *et al.*, 2014). It is assumed that the ubiquitin-binding domains of early endocytic factors bind and cluster ubiquitinated cargo, thereby selecting them for internalization and entry into the endosomal system (MacGurn *et al.*, 2012; Weinberg and Drubin, 2012). Similarly, at the endosome, the endosomal sorting complexes required for transport machinery specifically sorts ubiquitinated cargo proteins into intralumenal vesicles, a process called multivesicular body (MVB) biogenesis. Cargo proteins are subsequently degraded upon fusion of the MVB with the lysosome (Li and Kane, 2009; MacGurn *et al.*, 2012).

In *Saccharomyces cerevisiae*, PM protein ubiquitination and targeting for endocytosis is primarily mediated by Rsp5, the sole yeast member of the Nedd4 family of HECT-type E3 ubiquitin ligases. All members of the Nedd4 family contain two to four WW domains that bind specifically to proline-rich PPxY (PY) motifs (Harvey and Kumar, 1999; Boase and Kumar, 2015). Because many Nedd4-family substrates lack PY motifs, their indirect recognition relies on PY motif–containing soluble or membrane-bound adaptor proteins. A prominent group of soluble adaptor proteins is the family of α-arrestins, which is present in all eukaryotes except plants, with 6 identified members in mammals and 14 in yeast (Alvarez, 2008; Lin *et al.*, 2008; Piper *et al.*, 2014). α-Arrestins belong to the arrestin clan, which is defined by the presence of an arrestin core domain with N- and C-terminal arrestin folds. The arrestin clan also includes the visual arrestins, β-arrestins, and Vps26-like proteins (Aubry and Klein, 2013). A common feature of the α-arrestins is the presence of a large N- or C-terminal extension domain containing PY motifs that mediate the interaction with HECT-type ubiquitin ligases (Alvarez, 2008; Lin *et al.*, 2008; Kommaddi and Shenoy, 2013). The physiological role of human α-arrestins (ARRDC1 through ARRDC5 and TXNIP) is still poorly characterized, although initial studies suggested a role as ubiquitin ligase adaptors in ubiquitination and endocytic degradation of G protein–coupled receptors (GPCRs) and integrin β4 (Draheim *et al.*, 2010; Nabhan *et al.*, 2010; Patwari *et al.*, 2011; Shea *et al.*, 2012).

α-Arrestins are best characterized in *S. cerevisiae*, where their major role appears to be the recruitment of Rsp5 to PM nutrient transporters, causing their ubiquitination and endocytosis (Becuwe *et al.*, 2012; MacGurn *et al.*, 2012). However, roles at the Golgi and the endosome, as well as for endocytosis of GPCRs, have also been proposed (Herrador *et al.*, 2010; O'Donnell *et al.*, 2010; Becuwe *et al.*, 2012; Alvaro *et al.*, 2014; Becuwe and Leon, 2014). Yeast α-arrestins, hereafter referred to as arrestin-related trafficking adaptors (ARTs), include Bul1,2,3 (Merhi and Andre, 2012; Novoselova *et al.*, 2012), Spo23 (Aubry and Klein, 2013), and Art1 through Art10 (Lin *et al.*, 2008; Nikko and Pelham, 2009). Most ARTs have the ability to target multiple different cargo proteins under different conditions. For example, Art1 (also referred to as Ldb19) specifically regulates the endocytic degradation of the arginine permease Can1, the methionine permease Mup1, and the lysine permease Lyp1 (Lin *et al.*, 2008). In addition, it acts in concert with other ARTs to regulate the tryptophan permease Tat2, the uracil permease Fur4 (Nikko and Pelham, 2009), the α-factor receptor Ste2 (Alvaro *et al.*, 2014) and the a-factor receptor Ste3 (Prosser *et al.*, 2015), and is required for the recognition and degradation of numerous misfolded PM proteins upon heat stress (Zhao *et al.*, 2013). Similarly, individual cargo proteins can be targeted by multiple ARTs under different conditions (Lin *et al.*, 2008; Alvaro *et al.*, 2014). This high level of cross-connectivity enables the ART-Rsp5 network to tightly regulate the abundance of substrate proteins at the PM but raises the conundrum of how individual cargo proteins are targeted and how specificity is generated.

The mechanism by which α-arrestins bind to cargo proteins is unknown. Although they contain the arrestin core domain that is used by β-arrestins for binding to phosphorylated GPCRs, it is unclear whether cargo recognition by α-arrestins follows similar principles (Aubry *et al.*, 2009). Endocytic degradation of PM transporters by the ARTs has been shown to depend on poorly understood features of either the N- or the C-terminal cytoplasmic tail of the target protein, depending on the recognizing ART and the condition that triggers degradation (Lin *et al.*, 2008; Crapeau *et al.*, 2014). Several studies propose that substrate binding converts PM

transporters into an activated conformational state, which acts as a signal for degradation (Cain and Kaiser, 2011; Keener and Babst, 2013; Ghaddar *et al.*, 2014). However, there is no comprehensive model of the molecular features that contribute to ART binding to activated PM transporters.

Among the most frequently used model cargoes for endocytosis and endosomal trafficking is the high-affinity methionine permease Mup1. Mup1 contains 12 transmembrane domains (TMDs) and is a member of the APC superfamily (Gournas *et al.*, 2016). It localizes to the PM in the absence of its substrate, methionine. On methionine stimulation, Mup1 is rapidly ubiquitinated, endocytosed, and degraded in an Rsp5- and Art1-dependent manner (Menant *et al.*, 2006; Lin *et al.*, 2008; Keener and Babst, 2013).

In this study, we show that the recognition of Mup1 by Art1 upon methionine stimulation depends on the acidic patch, a sequence in the cytosolic N-terminus of Mup1. Mutations in the acidic patch block Mup1 ubiquitination and endocytosis but can be suppressed by mutations in the C-terminal domain of Art1, suggesting a functional (physical) relationship between both regions.

RESULTS

An unbiased mutagenesis screen reveals a role of the Mup1 N-tail in endocytic down-regulation

Endocytosis and vacuolar trafficking of PM transporters in yeast depend on cargo ubiquitination via the ubiquitin ligase Rsp5 (Piper *et al.*, 2014). Rsp5 is recruited to cargo proteins through the action of ART adaptor proteins (Lin *et al.*, 2008). The methionine transporter Mup1 is rapidly endocytosed after methionine stimulation, which is initiated by Art1-dependent ubiquitination of Mup1 by Rsp5 (Lin *et al.*, 2008). However, little is known about how Art1 recognizes Mup1 and how Mup1 is selected and targeted for endocytic degradation. We decided to isolate Mup1 mutants that are not endocytosed after methionine treatment to get a more comprehensive view of these mechanisms. To achieve this, we designed an unbiased genetic screen in which we fused green fluorescent protein (GFP) and the histidine biosynthetic enzyme His3 to Mup1 (Figure 1A). This chimeric construct restores histidine prototrophy (His+) in *his3Δ* cells (Figure 1B). However, upon overexpression of *ART1* from the Tet-Off promoter and addition of methionine to the medium, the fusion construct is degraded in the vacuole and the cells become histidine auxotrophs (His–; Figure 1, A and B). Overexpression of *ART1* was necessary to achieve stringent selection, most likely because the His3 fusion protein shows slower endocytic kinetics (Supplemental Figure S1). By mutagenizing Mup1 and plating the cells on medium with methionine and without histidine, we screened for Mup1 mutants that are not degraded after methionine stimulation. These mutants should be His+. We identified three individual single–amino acid substitutions in Mup1 that restore growth on medium lacking histidine in the presence of methionine even upon overexpression of *ART1*—D43N, G47S, and Q49R—of which Q49R showed the strongest effect (Figure 1C and Supplemental Figure S1). Endocytosis of Mup1-GFP leads to sorting of the fusion protein off the PM into the vacuole. Because GFP is resistant to vacuolar proteases, this causes accumulation of GFP signal in the vacuolar lumen. We took advantage of this and analyzed the phenotype of the Q49R mutation by microscopy. Whereas wild-type Mup1-GFP was completely endocytosed and sorted to the vacuole after a 90 min treatment with methionine, Mup1(Q49R)-GFP remained stable at the PM over the same time period, confirming strongly reduced endocytosis (Figure 1D). Of interest, all three mutated residues cluster in the cytosolic N-terminal tail of Mup1 (Figure 1E), suggesting an important role for the Mup1 N-tail in
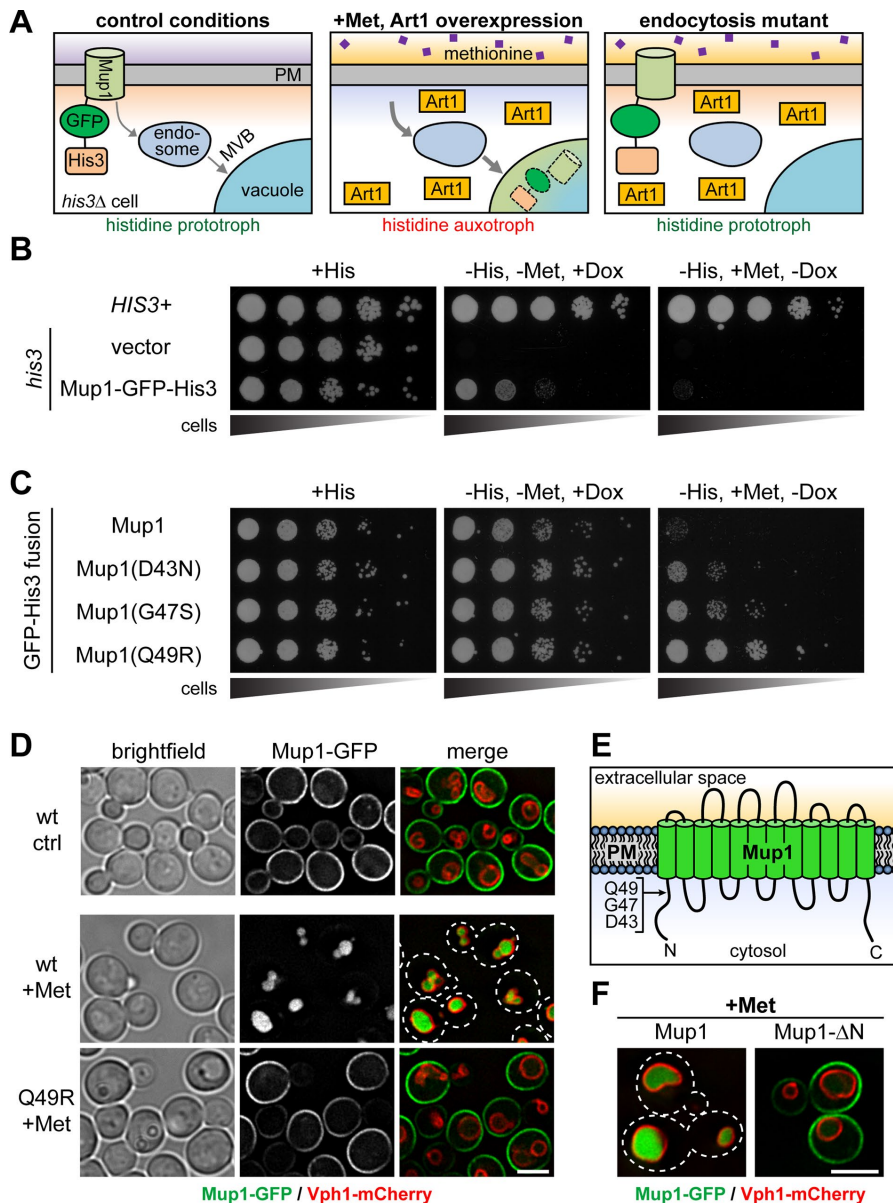
FIGURE 1: Identification of mutations that block Mup1 degradation by an unbiased mutagenesis screen. (A) Principle of the mutagenesis screen. Yeast cells lacking the histidine biosynthesis enzyme His3 gain histidine prototrophy by expression of Mup1-GFP-His3. On methionine stimulation and Art1 overexpression, the construct is turned over via endocytosis, sorting, and trafficking through the MVB pathway, causing the cells to return to histidine auxotrophy. Mutations that block endocytosis prevent degradation of the chimeric construct and allow growth in the absence of histidine even upon methionine stimulation. (B) Yeast cells expressing Art1 from the Tet-Off promoter were transformed with the indicated constructs, and serial 10-fold dilutions were spotted on synthetic medium plates containing or lacking histidine and methionine, as indicated. Medium lacking histidine was supplemented with 1 mM 3-AT, an inhibitor of His3, to enhance stringency. Doxycycline was added to the medium to a final concentration of 2.5 µg/ml to shut down expression of Art1. A strain with *HIS3*-marked Vph1-mCherry integrated into its genome served as the *HIS3*+ control. (C) Wild-type cells expressing Art1 from the Tet-Off promoter and the indicated mutated variants of Mup1-GFP-His3 were grown as described in B. Plates lacking histidine contain 5 mM 3-AT. (D) Fluorescence microscopy analysis of integrated Mup1-GFP and Mup1(Q49R)-GFP in wild-type yeast cells. The cells were grown to mid log phase in synthetic medium at 30°C and imaged before (ctrl) or after (+Met) 90 min 20 µg/ml methionine treatment, as indicated. Dashed lines represent cell outlines. Scale bar, 2.5 µm; vacuolar marker: Vph1-mCherry. (E) Cartoon of the PM 12-TMD methionine permease Mup1 depicting the location of Q49R, G47S, and D43N mutations. (F) Yeast cells expressing GFP-tagged Mup1 or a Mup1 deletion mutant lacking residues 17–56 of the 60 amino acid–long N-tail were grown to mid log phase in synthetic medium at 30°C and subjected to fluorescence microscopy after treatment with 20 µg/ml methionine for 90 min. Dashed lines indicate cell outlines. Scale bar, 2.5 µm; vacuolar marker: Vph1-mCherry.

endocytic degradation. Consistently, deleting a large portion of the N-tail (Mup1-ΔN) strongly blocked methionine-induced vacuolar sorting of Mup1 (Figure 1F). This observation is in agreement with a previous study from our group in which we demonstrated that Art1 recognizes an unknown element in the N-terminal cytosolic tail of Can1 (Lin et al., 2008).

Two distinct regions of the Mup1 N-terminal tail are critical for endocytic down-regulation

We decided to map more carefully the regions in the 60–amino acid N-terminal cytosolic tail of Mup1 that are important for endocytic down-regulation. We therefore generated a collection of GFP-tagged Mup1 mutants, each having 5 consecutive amino acids of the N-terminal tail replaced with alanines. We were unable to express a mutant in which amino acids 2–5 were mutated (unpublished data). Hence the covered region starts at the sixth amino acid and ends at the first transmembrane domain (TMD1). We analyzed each mutant for methionine-induced endocytosis by fluorescence microscopy and measured the effectiveness of sorting by determining the ratio of vacuolar to total cell GFP fluorescence. Strikingly, mutating two regions (26–30 and 41–55) strongly blocked methionine-induced degradation of Mup1, whereas mutating other residues had little to no effect (Figure 2, A and B, and Supplemental Figure S2).

Because GFP is stable in the yeast vacuole, degradation of Mup1-GFP can be assayed by Western blotting for the loss of full length Mup1-GFP and the concomitant accumulation of free GFP. The results of this degradation assay recapitulate the results of the fluorescent microscopy endocytosis assay, and mutating either region 26–30 or 41–55 stabilized Mup1-GFP in the presence of methionine (Figure 2C). These findings are in agreement with our results from the mutagenesis screen, as D43, G47, and Q49 all reside within the region 41–55. Yet the identification of a second region (26–30) was unexpected. We conclude that endocytosis of Mup1 requires two distinct regions of the cytosolic N-tail. Thus we set out to elucidate the molecular relevance of both regions for Mup1 endocytosis.

Rsp5 ubiquitinates Mup1 at lysines 27 and 28

We first investigated the region between residues 26 and 30, which contains two of the four lysine residues of the Mup1 N-tail (Figure 3A). Thus we asked whether Rsp5 ubiquitinates Mup1 at lysines 27 and 28. In
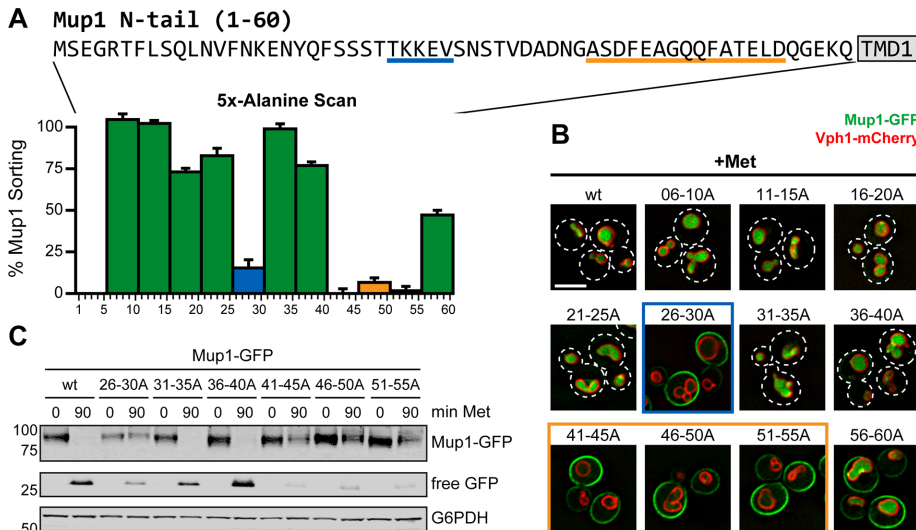
FIGURE 2: Two regions in the Mup1 N-terminal cytosolic tail are critical for endocytic down-regulation. (A) Top, sequence of the cytosolic N-tail (residues 1–60) of the yeast methionine transporter Mup1. The two regions critical for endocytosis are underlined. Bottom, a collection of GFP-tagged Mup1 mutants was stably integrated into yeast cells expressing Vph1-mCherry as vacuolar marker. In each mutant, five consecutive residues of the N-tail were mutated to alanines. Cells were grown to mid log phase in synthetic medium at 30°C, stimulated with 20 µg/ml methionine for 90 min, and analyzed by fluorescence microscopy. Average Mup1 sorting was calculated as the ratio of vacuolar GFP to total cell GFP and normalized to wild type before (0% sorting) and after methionine stimulation (100% sorting). The numbers below each bar of the graph correspond to the position of the substituted residues within Mup1. Error bars indicate SD between fields. (B) Representative images from cells quantified in A. Cells expressing GFP-tagged Mup1 or the indicated Mup1 alanine substitutions were grown to mid log phase in synthetic medium at 30°C and subjected to fluorescence microscopy after treatment with methionine for 90 min. A complete set of images is shown in Supplemental Figure S2. Dashed lines indicate cell outlines. Scale bar, 2.5 µm; vacuolar marker: Vph1-mCherry. (C) Yeast cells expressing GFP-tagged Mup1 or the indicated Mup1 alanine substitutions were grown to mid log phase in synthetic medium at 30°C and stimulated with 20 µg/ml methionine. Equal volumes of culture were harvested at the indicated time points after stimulation, and total cell lysates were prepared and analyzed by SDS–PAGE and immunoblot. G6PDH serves as a control for equal loading.

as Mup1 contains 19 lysine residues exposed to the cytosol.

Mup1 endocytosis depends on the acidic patch

We set out to decipher the mechanism by which the more C-terminal region of the Mup1 N-tail, between residues 41 and 55, regulates Mup1 degradation. We noticed that the region contains many negatively charged residues but is completely devoid of positive charges and hereafter refer to it as the "acidic patch." The charge distribution was particularly striking, as the strongest nondegradable Mup1 mutant that we isolated in our mutagenesis screen introduces a positive charge into the acidic patch by changing glutamine 49 to arginine. We reasoned that the acidic patch could be a charged interaction interface and that introducing positive charges could block this interaction. To test this idea, we individually mutated every amino acid within the acidic patch to arginine and tested all mutants for endocytic degradation by fluorescence microscopy. As before, the effectiveness of sorting was determined by the ratio of vacuolar to total cell GFP fluorescence (Figure 4, A and B, and Supplemental Figure S3). Of interest, we found that six of the 15 residues of the acidic patch had a strong effect on Mup1 degradation when they were converted to arginines. Of the remaining nine residues, five gave an intermediary phenotype, whereas mutating four had weak effects on Mup1 endocytosis. However, none of the mutants showed wild-type levels of Mup1 sorting. We decided to analyze more carefully three strong mutants that span the acidic patch: D43R, Q49R, and L54R. First, we verified the phenotype by immunoblot; all three mutants blocked degradation of Mup1-GFP (Figure 4C).

To test whether the acidic patch mutants block Mup1 endocytosis by affecting ubiquitination, we immunoprecipitated the GFP-tagged mutants from methionine-stimulated *doa4Δ* cells expressing Myc-ubiquitin (see earlier discussion). Probing the immunoprecipitates with Myc-antibody revealed that the acidic patch mutants are not ubiquitinated in the presence of methionine (Figure 4D).

To test the model that the acidic patch recruits Art1-Rsp5 and directs the specific ubiquitination of the nearby lysines K27 and 28, we designed an experiment to rule out any *trans* effects of the acidic patch mutants on other Mup1 molecules or on the ART-Rsp5 network more broadly. We coexpressed red fluorescent protein (RFP)–tagged, endocytosis-competent wild-type Mup1 and GFP-tagged Mup1 mutants in the same cells. Under control conditions, both constructs localize to the PM (Figure 4E). We noticed that the RFP signal in the bud was slightly weaker than the GFP signal, likely caused by slower maturation of the RFP fluorophore (Shaner *et al.*, 2008; Duwé *et al.*, 2015). Wild-type Mup1 was completely endocytosed within 90 min after methionine stimulation, regardless of the fluorophore. However, the GFP-tagged acidic patch mutants remained stable on the PM even in the presence of methionine, whereas the RFP-tagged wild-type Mup1 was efficiently sorted to

agreement with our hypothesis, mutating both residues to arginine blocked methionine-induced Mup1 degradation assayed by Western blot and fluorescence microscopy (Figure 3, B and C). Western blot analysis revealed a very small amount of remaining degradation in the K27,28R mutant, which could be completely eliminated by additionally mutating lysine 16 to arginine (Figure 3C). However, mutating lysine 16 alone had no observable effect on Mup1 degradation. We conclude that lysines 27 and 28 are critical for endocytosis of Mup1, most likely because they are ubiquitinated by Rsp5.

We also found that Mup1-GFP shifts to higher molecular weight within 5 min after methionine stimulation (Figure 3D). To test whether this shift is caused by ubiquitination, we coexpressed GFP-tagged Mup1 and Myc-tagged ubiquitin in a strain lacking the *DOA4* gene. *DOA4* encodes for the major deubiquitinating enzyme of the endomembrane system, and the *doa4Δ* background stabilizes ubiquitinated Mup1 (Amerik *et al.*, 2000; Katzmann *et al.*, 2001; Li *et al.*, 2015). Subsequently, we immunoprecipitated Mup1 after a brief methionine treatment and probed the immunoprecipitates with Myc antibodies. This revealed that the higher–molecular weight species of Mup1 are Myc positive, demonstrating that the shift in migration is indeed caused by ubiquitination (Figure 3E). Of importance, mutating lysines 27 and 28 to arginine blocked methionine-induced ubiquitination of Mup1. We therefore conclude that Rsp5 ubiquitinates Mup1 at lysines 27 and 28. This specificity is striking,

A

N-terminal cytosolic tail   TMD1

Mup1 MSEGRTFLSQLNVFN**K**ENYQFSSSTT**KK**EVSNSTVDADNGASDFEAGQQFATELDQGE**K**QLGIL...
                    16   27   59
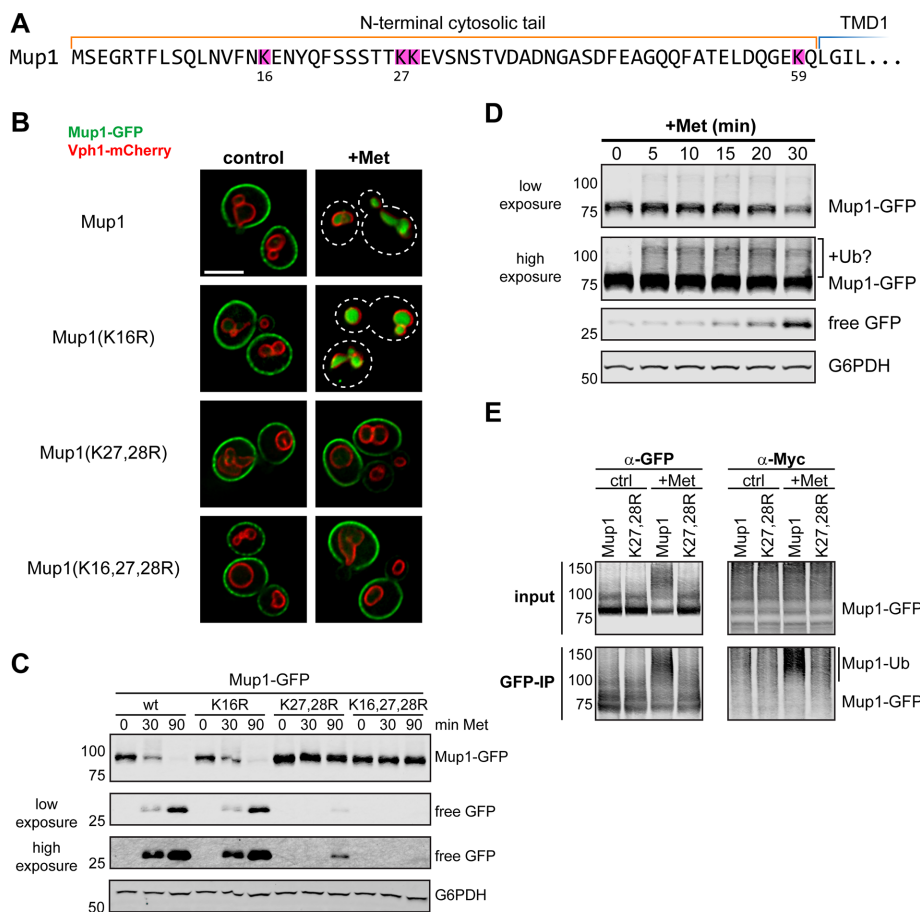
B

Mup1-GFP
Vph1-mCherry

C

D

E

FIGURE 3: Mup1 ubiquitination at lysines 27 and 28 initiates endocytic degradation. (A) Sequence of the N-terminal cytosolic tail of the yeast methionine transporter Mup1. Lysines are highlighted. (B) Fluorescence distribution of GFP-tagged Mup1 or Mup1 lysine mutants was analyzed in yeast cells expressing the vacuolar marker Vph1-mCherry. Cells were grown to mid log phase in synthetic medium at 30°C (control) and stimulated with 20 µg/ml methionine for 90 min (+Met). Dashed lines represent cell outlines. Scale bar, 2.5 µm. (C) Yeast cells expressing GFP-tagged Mup1 or Mup1 lysine mutants were grown to mid log phase in synthetic medium at 30°C and stimulated with 20 µg/ml methionine. Equal volumes of culture were harvested at the indicated time points after stimulation, and total cell lysates were prepared and analyzed by SDS–PAGE and immunoblot. G6PDH serves as a loading control. (D) Yeast cells expressing GFP-tagged Mup1 were grown to mid log phase in synthetic medium at 30°C and stimulated with 20 µg/ml methionine. At the indicated time points, all cellular processes were stopped by addition of TCA to 10% to the medium. Total cell lysates were prepared and analyzed by SDS–PAGE and immunoblot. G6PDH serves as a loading control. (E) Cells lacking Doa4 and coexpressing Myc-ubiquitin and Mup1-GFP or Mup1(K27,28R)-GFP were grown to mid log phase in synthetic medium at 30°C and mock treated (ctrl) or stimulated with 20 µg/ml methionine for 10 min (+Met). Native cell extracts were prepared and either analyzed by SDS–PAGE and immunoblot or used for GFP immunoprecipitation followed by SDS–PAGE and immunoblot.

The Mup1 N-terminal tail is necessary but not sufficient for Mup1 degradation

It is generally believed that PM transporters act as nutrient sensors and that substrate-induced conformational changes in each transporter molecule trigger its ubiquitination and degradation (Blondel et al., 2004; Jensen et al., 2009; Cain and Kaiser, 2011). For example, it was shown that substrate binding of the uracil permease Fur4 causes exposure of a degron that is not accessible in the ground state and thereby induces ubiquitination by Rsp5 and endocytic degradation (Keener and Babst, 2013). Our mutational analysis suggested that the Mup1 acidic patch might become exposed in the presence of methionine and act as a degron as well. To test for this, we generated a variant of Mup1 with two identical tandem tails at the N-terminus. We reasoned that this would cause constant exposure of any degron sequences in the N-tail and thus cause constitutive degradation of the fusion protein (Figure 5A). However, the fusion protein behaved like the wild-type Mup1, in that it was stable at the PM under control conditions and rapidly endocytosed upon methionine stimulation (Figure 5, B and C). We asked whether the fusion protein is stable because the additional degron is too far away from a second binding site or the membrane. We addressed this by mutating the acidic patch in either the membrane-proximal (native) or the membrane-distal (extra) tail and scoring these mutants for endocytosis upon methionine stimulation. In agreement with our hypothesis, the endocytosis of Mup1 depends on only the first acidic patch close to TMD1 (Figure 5, B and C), indicating that the additional tail is completely inactive for endocytic regulation. This demonstrates that the N-terminus of Mup1 is required but not sufficient for degradation, strongly arguing for a second degradation signal that is not part of the N-tail and functions in parallel to the acidic patch. In agreement with this, fusing the Mup1 N-terminus to GFP does not cause ubiquitination or degradation of the chimeric protein (Supplemental Figure S4). Furthermore, addition of a wild-type distal tail to a Mup1(K27,28R) mutant was unable to promote endocytosis, arguing that ubiquitination must occur close to the membrane-proximal acidic patch (Supplemental Figure S4). We conclude that the spacing between the acidic patch, lysines 27 and 28, and a currently unidentified feature (possibly the core of Mup1 or the PM) is critical for efficient ubiquitin-dependent endocytosis.

The Art1-regulated arginine permease Can1 also contains an acidic patch

The foregoing experiments demonstrate that endocytosis of Mup1 depends on an acidic patch between accessible lysines and TMD1.

the vacuole in the same cells (Figure 4E). This shows that cells expressing the acidic patch mutants are still able to efficiently endocytose wild-type Mup1. We therefore conclude that the acidic patch mutants must act in-*cis* and disrupt Art1-Rsp5–mediated ubiquitination of Mup1. These results also conclusively show that endocytosis of each Mup1 molecule is controlled individually: Art1-Rsp5 recruited to wild-type Mup1 cannot ubiquitinate nearby permeases, nor can nonubiquitinated permeases piggyback on the endocytic machinery assembled to internalize other ubiquitinated cargo.

Taken together, our data show that the Mup1 acidic patch is required for efficient ubiquitination and endocytic degradation in presence of methionine.
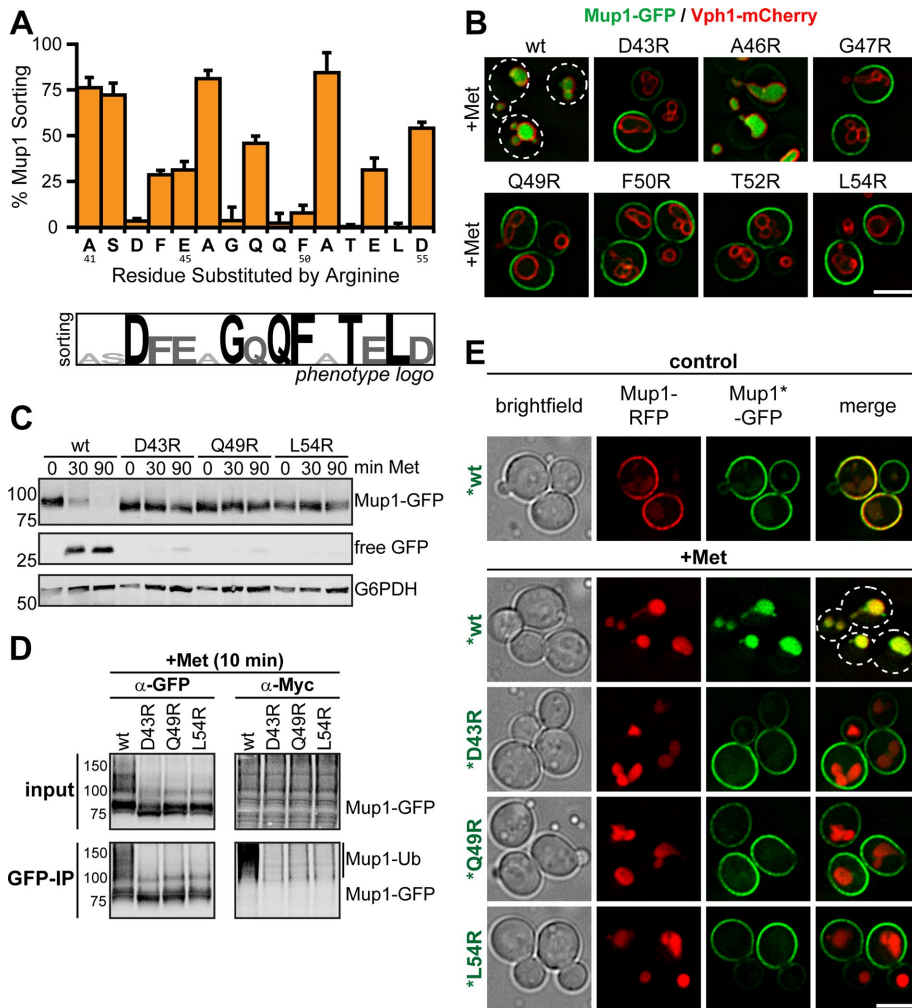
FIGURE 4: Mup1 degradation requires the acidic patch. (A) Top, yeast cells expressing Vph1-mCherry as vacuolar marker were transformed with a collection of GFP-tagged Mup1 mutants. In each mutant, one amino acid of the acidic patch was mutated to arginine. Cells were grown to mid log phase in synthetic medium at 30°C, stimulated with 20 µg/ml methionine for 90 min, and analyzed by fluorescence microscopy. Average Mup1 sorting was calculated as the ratio of vacuolar GFP to total cell GFP and normalized to wild type before (0% sorting) and after methionine stimulation (100% sorting). Error bars indicate SD between fields. Bottom, representation of the strength of the effect of each arginine substitution on Mup1 endocytosis as a "phenotype logo." Color and size of the substituted residue indicate the group to which it belongs (weak effects are represented in light gray and small letters, and strong effects are indicated by large letters and black). (B) Fluorescence distribution of GFP-tagged Mup1 or Mup1 acidic patch mutants grown as described in A. Images of all mutants are shown in Supplemental Figure S3. Vacuolar marker: Vph1-mCherry. Scale bar, 2.5 µm. (C) Yeast cells expressing GFP-tagged Mup1 or Mup1 acidic patch mutants were grown to mid log phase in synthetic medium at 30°C and stimulated with 20 µg/ml methionine. Equal volumes of culture were harvested at the indicated time points after stimulation, and total cell lysates were prepared and analyzed by SDS–PAGE and immunoblot. G6PDH serves as a loading control. (D) Cells lacking Doa4 and coexpressing Myc-ubiquitin and Mup1-GFP or the indicated GFP-tagged acidic patch mutants were grown to mid log phase in synthetic medium at 30°C and mock treated or stimulated with 20 µg/ml methionine for 10 min. Native cell extracts were prepared and either analyzed by SDS–PAGE and immunoblot or used for GFP immunoprecipitation followed by SDS–PAGE and immunoblot. (E) Yeast cells coexpressing RFP-tagged Mup1 (red) and the indicated GFP-tagged control or acidic patch mutants (green) were grown to mid log phase in synthetic medium at 30°C and subjected to fluorescence microscopy before (control) or after treatment with methionine for 90 min (+Met). Dashed lines indicate cell outlines. Scale bar, 2.5 µm.

Furthermore, our lab previously showed that Art1 recognizes an unknown feature in the N-terminus of the arginine permease Can1 (Lin et al., 2008). Thus we compared the sequences of the N-tails of Mup1 and Can1. Strikingly, we found that Can1 contains a mostly acidic region close to lysines and to the first TMD that resembled the acidic patch that we identified in Mup1 (Figure 6A). We therefore mutated this region by either mutating individual residues to arginine or multiple acidic residues to alanine and tested for Can1 endocytosis by assaying canavanine sensitivity. Canavanine is a toxic analogue of arginine that enters the cell via Can1. Thus the amount of active Can1 present at the PM directly correlates to the sensitivity to canavanine (Figure 6B; Lin et al., 2008; Shi et al., 2011). Intriguingly, mutating the acidic patch in Can1 renders the cells hypersensitive to canavanine (Figure 6C), most likely because endocytic degradation of the mutants is reduced. These results indicate that the presence of an acidic patch close to TMD1 is also important for endocytosis of Can1 and thus might be an extremely important shared feature of all Art1 targets.

Mup1 acidic patch mutants can be suppressed by mutations in Art1

The presence of the acidic patch in both Mup1 and Can1 suggested that this feature might mediate interaction with Art1. Art1 is a soluble 818–amino acid protein, with an arrestin fold from residues 135 to 397, an N-terminal phosphoregulatory domain, and a long C-terminal extension containing PY motifs at positions 678 and 689 (Lin et al., 2008; MacGurn et al., 2011). Therefore we addressed whether the acidic patch mutations interfere with the ability of Art1 to bind to Mup1. In an intracellular binding reaction, a reduction of binding affinity can often be compensated for by raising the amount of the binding partner. Thus we reasoned that if the acidic patch mutations reduce the affinity of Art1 for Mup1, overexpression of Art1 should be able to partially bypass this. Mup1 endocytosis requires both binding of Art1 and recruitment of Rsp5. We assumed that Art1 binding is the rate-limiting step, since Art1 is expressed at very low levels in cells (approximately 22 times lower than Rsp5; Kulak et al., 2014). Indeed, Art1 overexpression is sufficient to drive substantial endocytosis of wild-type Mup1-GFP even in the absence of methionine (Figure 7A). Furthermore, we found that overexpression of Art1 partially restored methionine-stimulated endocytosis of Mup1 D43R and F50R, which both show a strong block in cells expressing wild-type Art1 levels (Figures 4, A and B, and 7A). This suggests that mutations in the acidic patch interfere with the recruitment of Art1 to Mup1.
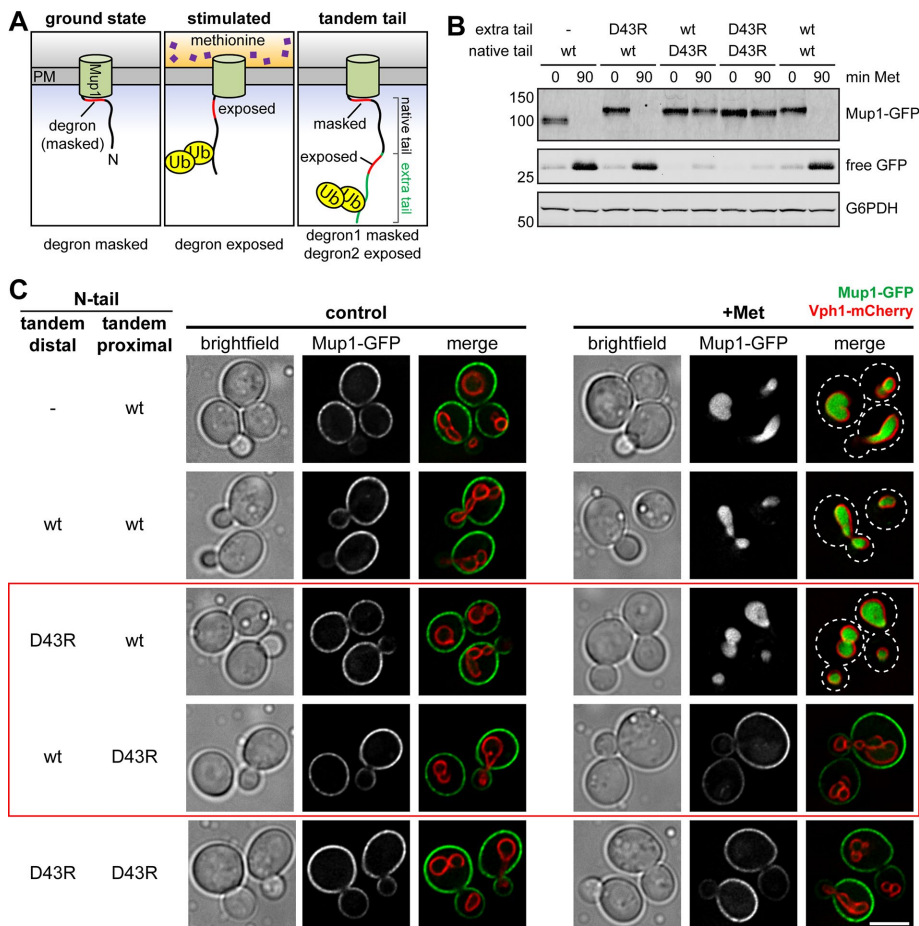
If the Mup1 acidic patch is indeed an Art1-interaction site, we reasoned that we should be able to identify mutations in Art1 that

FIGURE 5: The acidic patch is position specific. (A) Experimental rationale. In the degron model (Keener and Babst, 2013), permeases mask a degradation signal (degron) in the absence of their substrates. On transport or substrate binding, the permease enters an activated state and exposes the degron, causing its own ubiquitination and degradation. Under this model, tandemizing the N-terminal 60–amino acid tail of Mup1 should cause constant exposure of the additional degron in the extra tail, since the degron-binding site of the ground-state permease is occupied by the normal tail. (B) Yeast cells expressing GFP-tagged Mup1 tandem tail constructs were grown to mid log phase in synthetic medium at 30°C and stimulated with 20 µg/ml methionine. Equal volumes of culture were harvested at the indicated time points after stimulation, and total cell lysates were prepared and analyzed by SDS–PAGE and immunoblot. G6PDH serves as a loading control. (C) Yeast cells expressing GFP-tagged Mup1 tandem tail constructs were grown to mid log phase in synthetic medium at 30°C and subjected to fluorescence microscopy before (control) or after (+Met) treatment with methionine for 90 min. Dashed lines indicate cell outlines. Scale bar, 2.5 µm; vacuolar marker: Vph1-mCherry.

library of plasmids containing randomly mutagenized Art1* and screened the transformed cells for ethionine resistance. We recovered a mutant, Art1*Sup, that caused Mup1(Q49R) cells to become ethionine resistant but which in contrast had a reduced ability to promote ethionine resistance in wild-type cells (Figure 7D). Art1*Sup contained three mutations; we isolated each and found that Art1(R653C) alone was responsible for restoring Mup1 endocytosis.

We next used microscopy to verify that the Art1(R653C) mutation restores endocytosis of Mup1(Q49R)-GFP and that this phenotype is independent of the Art1* background. We indeed found that Art1(R653C) is able to promote endocytosis of Mup1(Q49R)-GFP when it is expressed from its endogenous promoter as the sole copy of Art1 (Figure 7E). However, the extent of endocytosis after methionine treatment is less than for wild-type Mup1-GFP expressing wild-type Art1. Art1(R653C) is also notably less effective than wild-type Art1 at promoting endocytosis of wild-type Mup1-GFP, indicating that R653C specifically suppresses the Mup1(Q49R)-GFP endocytic defect and is not a nonspecific hyperactivating mutation (Figure 7E). Consistently, cells expressing Art1(R653C) as their sole copy of Art1 are canavanine sensitive, suggesting that this mutation also reduces endocytosis of Can1 (Figure 7F). Art1 expression level, ubiquitination, and phosphorylation were unaffected by the R653C mutation; Art1(R653C) becomes hyperphosphorylated as normal during rapamycin treatment and hypophosphorylated after treatment with cycloheximide (Supplemental Figure S5; MacGurn et al., 2011).

We also noticed that the region of Art1 around R653 is conspicuously devoid of negative charges and contains additional positively charged arginines, suggesting that this C-terminal basic region of Art1 may be important for an electrostatic interaction

specifically suppress the effect of the Mup1 acidic patch mutations. To identify such a suppressor mutant, we took advantage of the toxic methionine analogue ethionine, which enters the cell through the methionine transporter Mup1 (Isnard et al., 1996; Santiago and Gardner, 2015). As with canavanine and Can1, the sensitivity to ethionine should directly correlate with the activity and PM localization of Mup1. Cells that do not express Mup1 are therefore resistant to ethionine, and cells expressing wild-type Mup1 are sensitive. Mutations that block Art1 phosphorylation at some or all of 10 N-terminal serines and/or threonines have been shown to cause Art1 hyperactivation (MacGurn et al., 2011). We expressed such a hyperactive Art1 allele, Art1*, from a Tet-Off promoter, which confers ethionine resistance because it causes constant vacuolar sorting of Mup1-GFP. Mup1(Q49R), however, remains stable at the PM despite overexpression of Art1*, causing cells to become ethionine sensitive (Figure 7, B and C). We transformed the Mup1(Q49R) mutant with a

with the Mup1 acidic patch. If Art(R653C) acts by removing a positive charge to compensate for the introduction of a positive charge in the acidic patch in the Q49R mutant, we reasoned we could suppress additional acidic patch mutants with other charge inversions in Art1. We generated the Art1(R660D) mutant and tested whether it restores endocytosis of any of the strong Mup1 acidic patch mutants (D43R, G47R, Q49R, F50R, T52R, or L54R). Remarkably, upon methionine stimulation, overexpression of Art1(R660D) specifically restored endocytosis for Mup1(D43R)-GFP, as Art1(R653C) did for Mup1(Q49R)-GFP (Figure 8A). Quantification of vacuolar GFP compared with total cellular GFP revealed that the Art1(R660D)/Mup1(D43R) combination is noticeably less efficient than the suppression observed for Art1(R653C)/Mup1(Q49R). However, in both cases, restoration of Mup1 sorting was allele specific (Figure 8, A and B). Taken together, the opposing charges of the Art1 C-terminal basic region and the Mup1 acidic patch suggest a direct interaction
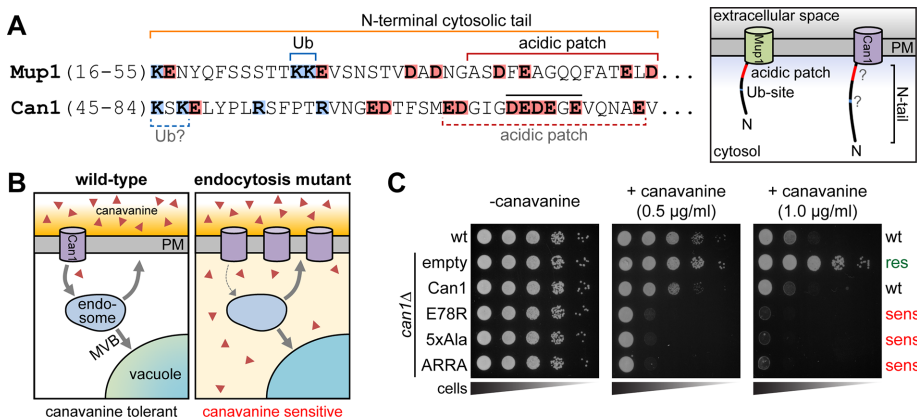
FIGURE 6: Can1 contains an acidic patch. (A) Left, comparison between the N-terminal cytosolic tails of Mup1 and Can1. TMD1 (not shown) begins at 61 in Mup1 and 93 in Can1. Right, representation of Can1 and Mup1 with the position and size of the acidic patch and the ubiquitination site drawn to scale. (B) Yeast cells turn over the PM arginine permease Can1 by endocytosis and vacuolar degradation. Mutations that block Can1 endocytosis stabilize the permease at the PM, causing hypersensitivity to canavanine, a toxic analogue of arginine that enters the cells via Can1. (C) Cells lacking a chromosomal copy of Can1 were transformed with plasmids expressing either wild-type Can1 or the following point mutants and scored for growth in the presence of canavanine: E78R, Can1(E78R); 5xAla, Can1(D73A,E74A,D75A,E76A,E78A); and ARRA, Can1(D73A,E74R,D75R,E76A). The mutated region is highlighted with a bar in A. Canavanine sensitivity phenotype is scored on the right; res, resistant; sens, sensitive; wt, wild type.

(Figure 8C). This is supported by the ability of mutations that remove positive charges from Art1 to allele-specifically suppress mutations that introduce positive charge into Mup1.

DISCUSSION

It has been known for many years that changes in nutrient availability trigger the degradation of PM transporters in yeast (Rotin *et al.*, 2000). Most transporters are ubiquitinated by a single E3 ligase, Rsp5, leading to the question of how specificity is encoded in this degradation system. The first clue came with the identification of 14 ART adaptor proteins that recruit Rsp5 to its substrates in an adaptor-cargo–specific manner (Lin *et al.*, 2008; Nikko and Pelham, 2009). However, ARTs were found to target multiple substrate proteins, and thus the identification of the ART-Rsp5 ubiquitin ligase network still did not explain the high specificity in the degradation pathway. The answer most likely lies in the molecular mechanism of the ART-substrate interaction and how recruitment of the ART-Rsp5 complex to cargo proteins is regulated. Here we present the first detailed analysis of an interaction between a permease and its cognate ART-Rsp5 ubiquitin ligase complex. We find that Art1-dependent endocytosis of Mup1 requires a multipart degradation signal, with 1) an extended acidic patch, 2) in close proximity to the membrane, and 3) with a precise distance to its target lysines, together referred to as the ART sorting signal.

First, in this study, we show that endocytic degradation of Mup1 requires an extended region in the N-tail between residues 41 and 55, which we term the acidic patch. As the name indicates, it is devoid of positive charges (R + K + H) and enriched for negatively charged residues (D + E). Either replacing charged residues with alanines or introducing positively charged arginines strongly blocks Mup1 endocytosis. Of interest, our arginine substitution approach revealed that not every residue of the acidic patch is equally important for efficient endocytosis. Instead, substituting several residues with arginine had only mild effects (Figure 4A). This is indicative of a structured region in which certain residues participate in binding to

the degradation machinery, but the irregular spacing of the critical acidic patch residues is not obviously consistent with an α-helical or a β-sheet fold.

Second, our tandem tails experiments show that the N-tail alone is insufficient for productive ubiquitination. Furthermore, adding a second wild-type N-tail to a Mup1 acidic patch mutant does not restore endocytosis. This strongly argues that Mup1 degradation heavily depends on proximity of the acidic patch to TMD1. This result is consistent with a model in which productive endocytosis requires multiple contacts between the Art1-Rsp5 complex and Mup1—one at the acidic patch, and a second, potentially between the Art1 arrestin fold and the Mup1 core (e.g., cytoplasmic loops or the TMDs).

Third, we observe extremely high specificity in the Mup1 ubiquitination site (Figure 3). We found that a distal, wild-type tandem tail could not restore endocytosis of the Mup1(K27,28R) mutant, indicating that those lysines can only be productively ubiquitinated when sufficiently close to the membrane-proximal acidic patch. Bolstering this line of reasoning, Mup1 has 19 lysine residues exposed to the cytoplasm, of which 4 are in the N-tail, 9 in cytoplasmic loops, and 6 in the C-tail. The strict requirement of lysines 27 and 28 in Art1-Rsp5–mediated, methionine-induced Mup1 endocytosis is in contrast to the widespread promiscuity of ubiquitin ligases, which show little lysine selectivity for most targets (Mattiroli and Sixma, 2014), and resembles instead the high lysine selectivity of other endocytic cargoes such as Fur4 and Gap1 (Keener and Babst, 2013; Crapeau *et al.*, 2014).

Despite the importance of the acidic patch for Mup1 sorting, it has no direct sequence conservation in other Art1 targets. Instead, we suspect that Art1-Rsp5 specificity arises from the combined effects of the tripartite ART sorting signal. Consistently, we showed that an acidic patch in Can1, matching our other criteria of proximity to TMD1 and with appropriately spaced lysines, is important for Can1 endocytosis (Figure 6).

In strong support of our model, in which the acidic patch interacts with the Art1-Rsp5 complex, we show that individual charge inversion mutations in the Mup1 acidic patch can be suppressed by opposite-charge inversion mutations in Art1, suggesting an electrostatic interaction between the two regions. Although α-arrestins lack the polar core in the arrestin domain that is used for cargo interactions in β-arrestins (Aubry *et al.*, 2009; Polekhina *et al.*, 2013), it has been proposed that α-arrestins use the arrestin domain for substrate binding as well (Qi *et al.*, 2014). Unexpectedly, both Art1 suppressor mutations, R653C and R660D, cluster downstream of the arrestin domain (residues 135–397) in the C-terminal domain, close to the PY motifs (678–682 and 689–692) that recruit Rsp5 (Lin *et al.*, 2008). This C-terminal extension domain can be found only in α-arrestins. It can be several hundred amino acids long, is located either N- or C-terminal of the core domain, and usually harbors the PY motifs (Lin *et al.*, 2008; Aubry and Klein, 2013). Judged by the large size, it is unlikely that the only function of the extension domain is the recruitment of the ubiquitin ligase. On the basis of our data, we conclude that a major novel function of the C-terminal domain of Art1 is to interact with the acidic patch of Mup1.
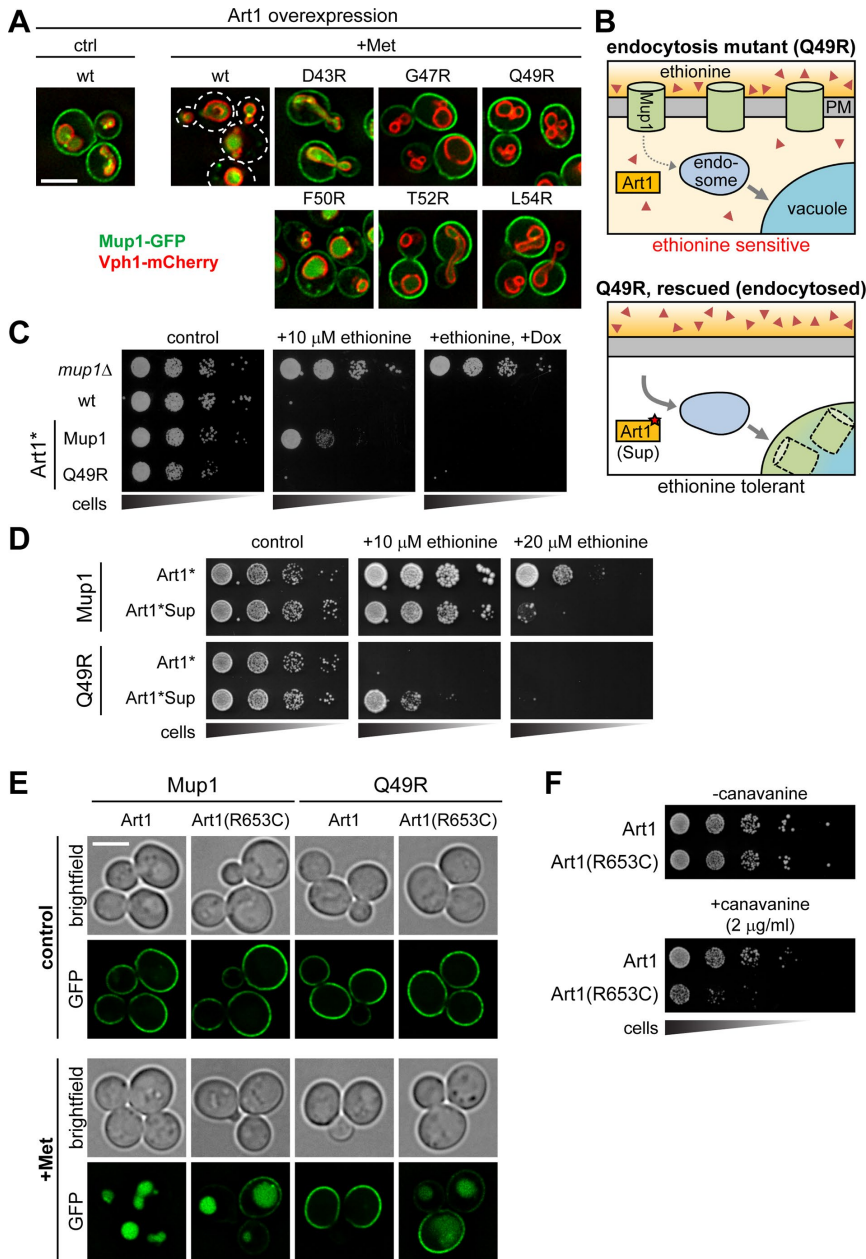
FIGURE 7: Identification of an Art1 mutant that restores endocytosis of Mup1(Q49R). (A) Yeast cells expressing GFP-tagged Mup1 acidic patch mutants and overexpressing Art1 from a single-copy plasmid and the Tet-Off promoter were grown to mid log phase in synthetic medium at 30°C, stimulated with 20 μg/ml methionine for 60 min if indicated (+Met), and subjected to fluorescence microscopy. Scale bar, 2.5 μm; vacuolar marker: Vph1-mCherry. (B) Ethionine is a toxic analogue of methionine that enters the cells via the PM methionine permease Mup1. Mutants that are defective for endocytic Mup1 degradation, such as Mup1(Q49R), accumulate Mup1 at the PM and are therefore sensitive to ethionine. Mutations in Art1 that restore vacuolar trafficking of Mup1(Q49R) reduce the amount of Mup1 at the PM and cause the cells to return to an ethionine-resistant state. (C) Serial 10-fold dilutions of cells expressing hyperactivated Art1 (Art1*; Art1(79,82–85,96,99, 100A); MacGurn et al., 2011) from the Tet-Off promoter were spotted on agar plates and scored for growth in the presence of ethionine. Doxycycline was added to a final concentration of 2.5 μg/ml to shut off overexpression of Art1. (D) Serial 10-fold dilutions of cells expressing Art1* or Art1*Sup from the Tet-Off promoter were spotted on agar plates and scored for growth in the absence or presence of 10 or 20 μM ethionine. Art1*Sup, Art1(79,82–85,96,99,100A,S253P,E445G, R563C). (E) Yeast cells lacking the chromosomal copy of *ART1* and expressing Art1 or Art1(R563C) from a single-copy plasmid under its own promoter were transformed with the indicated variants of Mup1-GFP. The cells were grown to mid log growth phase in synthetic medium at 30°C and stimulated with 20 μg/ml methionine for 90 min. Scale bar, 2.5 μm. (F) Yeast cells lacking the chromosomal copy of *ART1* and expressing Art1 or Art1(R653C) from a single-copy plasmid under its own promoter were scored for growth in the presence of canavanine.

However, our data suggest that this cannot be the only interaction between Mup1 and Art1-Rsp5. Of interest, studies on the interaction between GPCRs and β-arrestins revealed a bipartite binding mechanism: after GPCR phosphorylation by receptor kinases, the generated phosphocluster on the GPCR C-terminal tail directly interacts with positive charges of the arrestin core domain. Subsequently, a finger loop of the arrestin N-domain binds the TMDs of the GPCR core (Shukla et al., 2013, 2014; Kang et al., 2015). Similarly, the arrestin domain of Art1 could bind to the core of Mup1, whereas the Art1 C-terminal domain interacts with the Mup1 acidic patch. This can explain why the acidic patch needs to be close to the core of Mup1 in order to be functional.

On the basis of our genetic suppression analysis, the tandem tail experiment, and the binding mechanism known for β-arrestins, we propose that Art1 interacts with Mup1 at the acidic patch and an as-yet-unidentified second site and that the spacing between both interaction sites is important for Art1 function. Furthermore, the proximity of the Mup1 acidic patch to the ubiquitinated lysines and the proximity of the Art1 C-terminal basic region to the Rsp5-recruiting PY motifs made us wonder whether Art1 could use this interaction to orient the HECT domain of Rsp5 toward the target lysines in Mup1. This resembles the mechanism that RING-type ligases use to ubiquitinate their substrates (Budhidarmo et al., 2012). This would assign to Art1 a previously unknown direct involvement in cargo ubiquitination, but additional work is required to confirm this model. Taken together, we present a model in which Art1 engages Mup1 with at least two interaction sites and the C-terminal extension domain of Art1 directly interacts with the acidic patch of Mup1, thereby orienting Rsp5 favorably toward Mup1's lysines 27/28 (Figure 9).

MATERIALS AND METHODS

Yeast strains and growth conditions

All yeast strains used in this study are listed in Supplemental Table S1. Standard procedures were used for manipulation of yeast. Yeast deletion mutants were generated by homologous recombination. Double-deletion mutants were constructed by mating and tetrad dissection. Yeast strains were isogenic to SEY6210 or SEY6210.1. All plasmids derived from pRS305 were integrated into the *leu2* locus after plasmid digestion with *Afl*II. The functionality of stable Mup1 mutants was ensured by rescue of the synthetic growth defect of *mup1Δ met6Δ* double mutants (Supplemental Figure S6).
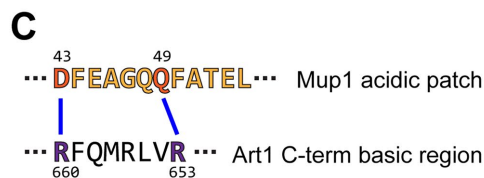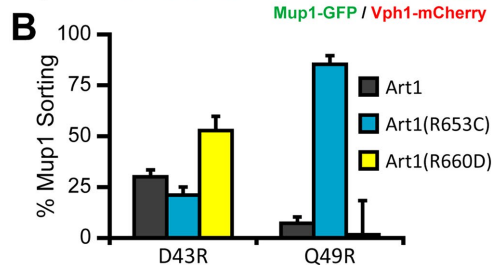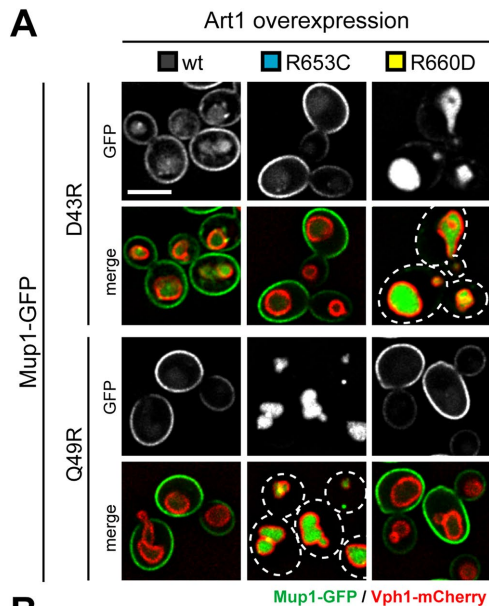
FIGURE 9: Model for Art1-mediated Mup1 recognition. In the absence of methionine, Mup1 is present in a ground state, and the acidic patch is inaccessible for Art1. In the presence of methionine, however, Mup1 adopts an activated state in which the ART sorting signal becomes exposed, causing Art1-mediated recruitment of Rsp5, Mup1 ubiquitination, and trafficking to the vacuole.

FIGURE 8: Multiple point mutations in Art1 allele specifically restore endocytosis of Mup1 acidic patch mutants. (A) Yeast cells expressing the indicated GFP-tagged Mup1 acidic patch mutants and carrying a single-copy plasmid overexpressing Art1, Art1(R653C), or Art1(R660D) from the Tet-Off promoter were grown to mid log growth phase in synthetic medium at 30°C and stimulated with 20 µg/ml methionine for 60 min. Dashed lines indicate cell outlines. Scale bar, 2.5 µm; vacuolar marker: Vph1-mCherry. (B) Cells were grown as described in A and analyzed by fluorescence microscopy. Average Mup1 sorting was calculated as the ratio of vacuolar GFP to total cell GFP and normalized to wild type before (0% sorting) and after methionine stimulation (100% sorting). Error bars indicate SD between fields. (C) Schematic representation of the Mup1 acidic patch region and the region in Art1 that harbors the suppressor mutations. Blue lines indicate which mutated residues in Art1 restore endocytosis of the respective acidic patch arginine substitution mutants in an allele-specific manner.

For the Mup1 degradation assay, yeast cells were grown in synthetic complete medium lacking methionine to mid log phase and did not reach saturation for at least 16 h. Degradation of Mup1 was triggered by addition of methionine to a final concentration of 20 µg/ml. All strains were grown at 30°C.

Plasmids and cloning

Standard procedures were used for cloning and amplification of plasmids. Restriction enzymes were purchased from NEB (New England Biolabs, Ipswich, MA). All plasmids used in this study are listed in
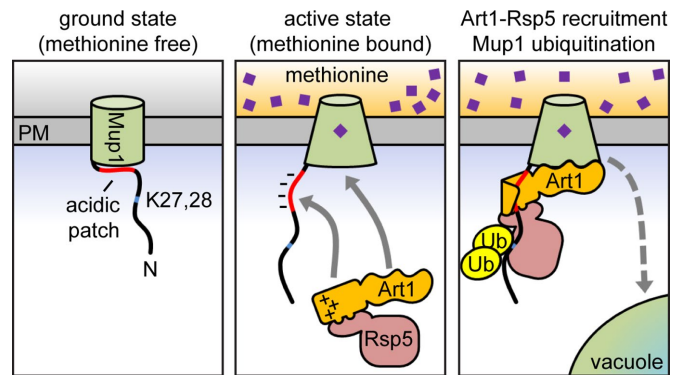
Supplemental Table S2. PCRs were performed using Phusion DNA polymerase (Thermo Fisher Scientific, Waltham, MA) according to the manufacturer's instructions. KOD DNA-polymerase (EMD Millipore, Billerica, MA) was used for site-directed introduction of mutations according to the manufacturer's instructions. Supplemental Table S3 lists oligonucleotides used for cloning and strain construction.

Random mutagenesis screen

Random mutagenesis was performed by error-prone PCR using Taq polymerase and buffer-EP (10 mM Tris, pH 8.3, 50 mM KCl, 1.5 mM $MgCl_2$, 1 mM dCTP, dTTP, 0.2 mM dATP, dGTP, 0.1 mM $MnCl_2$, 3% dimethyl sulfoxide, 1 µM F&R primers, 200 ng/ml template) with hot start at 94°C for 2 min, 25 cycles (94°C for 30 s, 54°C for 30 s, 68°C for 2 min/kb), and 68°C for 10 min, followed by lithium acetate yeast transformation at a 10:1 insert:vector molar ratio with 250 ng of linearized vector per 1.5 OD of cells. Recombination was achieved by gap repair with 200–base pair overhanging 5′ and 3′ homology. *MUP1-GFP-HIS3* was amplified with EG7F and EG19R from pEG114 and transformed with *Eag*I-cut pEG115. *ART1*(8A) was amplified with EG141F and EG142R from pTK177 and transformed with *Pst*I-cut pCM189. Transformations were allowed to recover 4 h in YPDA (1% yeast extract, 2% peptone, 2% dextrose, 20 µg/ml adenine) before plating. *MUP1* mutagenesis was performed in TKY072 expressing pTK138 and plated on –URA –LEU –HIS medium containing 10 mM 3-amino-1,2,4-triazole (3-AT; Sigma-Aldrich, St. Louis, MO) and 164 µg/ml methionine. *ART1* mutagenesis was performed in YEG131 and plated on –URA –MET medium containing 10 µM D/L-ethionine (TCI, Tokyo, Japan). Colonies were retested for HIS+ growth by spot assay followed by visual screening for PM GFP signal or for resistance to ethionine by spot assay ± 2.5 µg/ml doxycycline (MPBio, Santa Ana, CA). Plasmids encoding candidate *mup1* and *art1* mutants were isolated for further analysis by miniprep after glass bead lysis.

Microscopy, data analysis, and image processing

Microscopy was performed using 1) a DeltaVision RT system (Applied Precision, Issaquah, WA) equipped with a 100× objective, a DeltaVision RT Standard Filter Set (fluorescein isothiocyanate [FITC] for GFP and RD-TR-Cy3 for mCherry/RFP), and a Photometrics CoolSNAP HQ camera (Photometrics, Tucson, AZ), or 2) a DeltaVision RT system equipped with a DV Elite complementary metal-oxide semiconductor camera, a 100× objective, and a DV Light SSI 7 Color illumination system with Live Cell Speed Option (FITC for

GFP and tetramethylrhodamine isothiocyanate for mCherry/RFP). Image acquisition and deconvolution were performed using the provided DeltaVision software (softWoRx 3.5.1: aggressive, 10 iterations; softWoRx 6.5.2: conservative, five iterations; Applied Precision). Images were adjusted for brightness and contrast.

Mup1-GFP sorting was quantified from unprocessed images with an in-house algorithm written in Python 2.7 (Python Software Foundation, Wilmington, DE). Briefly, cells were identified from bright-field images using a Laplacian of Gaussian kernel (Jones et al., 2001) to detect cell edges, and vacuoles were detected from Vph1-mCherry images by Otsu thresholding (van der Walt et al., 2014). After background correction, GFP signal was measured in the whole cell and in the vacuole. Sorting was calculated as the vacuolar-GFP signal divided by the total cell GFP signal, normalized between 0% sorting (vacuolar/total GFP in cells expressing wild-type Mup1-GFP without methionine) to 100% sorting (vacuolar/total GFP in cells expressing wild-type Mup1-GFP after 90-min treatment with methionine). An average of 50 cells were scored for each field; to compensate for slight variations in the number of cells in different fields, sorting was calculated for each field and averaged across six fields collected from two or more experiments. Additional details and Python code are available upon request.

Generation of GFP nanobody resin
Escherichia coli cells (BL-21) were grown in Terrific Broth at 37°C, and the C-terminally hexahistidine-tagged GFP-nanobody GBP1 (Kirchhofer et al., 2010) was expressed by addition of isopropyl-β-D-thiogalactoside to a final concentration of 250 µM and subsequent incubation overnight at 18°C. The cells were pelleted, resuspended in lysis buffer (40 mM Tris HCl, pH 7.5, 5% glycerol, 300 mM NaCl, 10 mM imidazole) supplemented with 1 mM phenylmethylsulfonyl fluoride (PMSF) and lysed by sonication. The cell lysate was cleared by centrifugation and bound to TALON Metal Affinity Resin (Takara Bio, Mountain View, CA). After washing, bound protein was eluted with lysis buffer containing 250 mM imidazole and dialyzed into phosphate-buffered saline (PBS). The purified nanobody was coupled to NHS-activated Sepharose 4 FF (GE Healthcare, Wilkes-Barre, PA) for 4 h at room temperature in PBS according to the manufacturer's instructions.

Total cell extracts for SDS–PAGE
Total cell lysates were prepared by incubating 6–9 OD of cells in 10% trichloroacetic acid (TCA) on ice for 1 h. The cells were washed twice in acetone, bead-beat in 100 µl of 2× urea buffer (50 mM Tris HCl, pH 7.5, 8 M urea, 2% SDS, 1 mM ethylenediaminetetraacetic acid [EDTA]) for 5 min, and incubated at 42°C for 5 min. Bead beating and heating were repeated after addition of 100 µl of 2× sample buffer (150 mM Tris HCl, pH 6.8, 7 M urea, 10% SDS, 24% glycerol, bromophenol blue) supplemented with either 10% 2-mercaptoethanol or 100 mM dithiothreitol (DTT).

Western blotting and antibodies
Samples were run on 6, 9, 11, or 13% polyacrylamide gels and transferred to supported 0.45-µm nitrocellulose membranes (GE Healthcare). Membranes were blocked with 5% fat-free milk in Tris-buffered saline/Tween-20. Antibodies used were rabbit anti–glucose-6-phosphate dehydrogenase (G6PDH; A9521; Sigma-Aldrich), mouse monoclonal anti-GFP (11814460001; Roche Diagnostics, Rotkreuz, Switzerland), rabbit anti-GFP (TP401; Torrey Pines Biolabs, Secaucus, NJ), mouse monoclonal anti–FLAG-M2 (F1804; Sigma-Aldrich), 800CW goat anti-rabbit (926-32211; LI-COR Biosciences, Lincoln, NE), 800CW goat anti-mouse (926–32210; LI-COR

Biosciences), 680LT goat anti-rabbit (926–68021; LI-COR Biosciences), and 680LT goat anti-mouse (926-68021; LI-COR Biosciences). Membranes were scanned using an Odyssey CLx imaging system and analyzed using the Image Studio Lite 4.0.21 software (LI-COR Biosciences). For Mup1 degradation assays, full-length Mup1-GFP and free GFP were detected with mouse monoclonal anti-GFP antibody on a single membrane and brightness and contrast adjusted separately due to differences in transfer efficiency.

Ubiquitination assay
The ubiquitination assay was adapted from Li et al. (2015) with some modifications. In brief, cells were grown to early log phase in synthetic medium, and expression of Myc-ubiquitin was induced with 100 µM CuSO$_4$ followed by 4–6 h of induction. Ubiquitination of Mup1 was induced by adding methionine to a final concentration of 20 µg/ml. After 15 min, 40 OD of cells were harvested, washed with water, and snap frozen in liquid nitrogen. The frozen pellet was resuspended in 450 µl RIPA buffer (50 mM Tris HCl, pH 7.6, 150 mM NaCl, 20 mM NaF, 1 mM EDTA, 0.5 mM ethylene glycol tetraacetic acid) supplemented with 1 mM DTT, 1 mM PMSF, and cOmplete protease inhibitor (Sigma-Aldrich), and 20 mM N-ethylmaleimide. Cell extracts were prepared by bead beating twice for 6 min each at 4°C. Membranes were solubilized by nutating for 30 min at 4°C after addition of 50 µl of 10% NP-40 and 5% deoxycholate in RIPA buffer. The lysates were diluted 1:1 with RIPA buffer, and insoluble material was removed by two rounds of centrifugation at 16,100 × g and 4°C for 12 min. The cleared lysate was incubated with 25 µl of GFP-nanobody resin at 4°C for 4 h. Afterward, the resin was washed three times with 0.1% NP-40 and 0.05% deoxycholate in RIPA buffer, and bound proteins were eluted by addition of equal volumes of 2× urea buffer and 2× sample buffer, followed by incubation at 42°C for 5 min.

REFERENCES
Alvarez CE (2008). On the origins of arrestin and rhodopsin. BMC Evol Biol 8, 222.

Alvaro CG, O'Donnell AF, Prosser DC, Augustine AA, Goldman A, Brodsky JL, Cyert MS, Wendland B, Thorner J (2014). Specific alpha-arrestins negatively regulate Saccharomyces cerevisiae pheromone response by down-modulating the G-protein-coupled receptor Ste2. Mol Cell Biol 34, 2660–2681.

Amerik AY, Nowak J, Swaminathan S, Hochstrasser M (2000). The Doa4 deubiquitinating enzyme is functionally linked to the vacuolar protein-sorting and endocytic pathways. Mol Biol Cell 11, 3365–3380.

Aubry L, Guetta D, Klein G (2009). The arrestin fold: variations on a theme. Curr Genomics 10, 133–142.

Aubry L, Klein G (2013). True arrestins and arrestin-fold proteins: a structure-based appraisal. Prog Mol Biol Transl Sci 118, 21–56.

Becuwe M, Herrador A, Haguenauer-Tsapis R, Vincent O, Leon S (2012). Ubiquitin-mediated regulation of endocytosis by proteins of the arrestin family. Biochem Res Int 2012, 242764.

Becuwe M, Leon S (2014). Integrated control of transporter endocytosis and recycling by the arrestin-related protein Rod1 and the ubiquitin ligase Rsp5. Elife 3.

Blondel MO, Morvan J, Dupre S, Urban-Grimal D, Haguenauer-Tsapis R, Volland C (2004). Direct sorting of the yeast uracil permease to the endosomal system is controlled by uracil binding and Rsp5p-dependent ubiquitylation. Mol Biol Cell 15, 883–895.

Boase NA, Kumar S (2015). NEDD4: the founding member of a family of ubiquitin-protein ligases. Gene 557, 113–122.

Budhidarmo R, Nakatani Y, Day CL (2012). RINGs hold the key to ubiquitin transfer. Trends Biochem Sci 37, 58–65.

Cain NE, Kaiser CA (2011). Transport activity-dependent intracellular sorting of the yeast general amino acid permease. Mol Biol Cell 22, 1919–1929.

Crapeau M, Merhi A, Andre B (2014). Stress conditions promote yeast Gap1 permease ubiquitylation and down-regulation via the arrestin-like Bul and Aly proteins. J Biol Chem 289, 22103–22116.

Draheim KM, Chen HB, Tao Q, Moore N, Roche M, Lyle S (2010). ARRDC3 suppresses breast cancer progression by negatively regulating integrin beta4. Oncogene 29, 5032–5047.

Duwé S, De Zitter E, Gielen V, Moeyaert B, Vandenberg W, Grotjohann T, Clays K, Jakobs S, Van Meervelt L, Dedecker P (2015). Expression-enhanced fluorescent proteins based on enhanced green fluorescent protein for super-resolution microscopy. ACS Nano 9, 9528–9541.

Feyder S, De Craene JO, Bar S, Bertazzi DL, Friant S (2015). Membrane trafficking in the yeast Saccharomyces cerevisiae model. Int J Mol Sci 16, 1509–1525.

Ghaddar K, Merhi A, Saliba E, Krammer EM, Prevost M, Andre B (2014). Substrate-induced ubiquitylation and endocytosis of yeast amino acid permeases. Mol Cell Biol 34, 4447–4463.

Gournas C, Prevost M, Krammer EM, Andre B (2016). Function and regulation of fungal amino acid transporters: insights from predicted structure. Adv Exp Med Biol 892, 69–106.

Harvey KF, Kumar S (1999). Nedd4-like proteins: an emerging family of ubiquitin-protein ligases implicated in diverse cellular functions. Trends Cell Biol 9, 166–169.

Herrador A, Herranz S, Lara D, Vincent O (2010). Recruitment of the ESCRT machinery to a putative seven-transmembrane-domain receptor is mediated by an arrestin-related protein. Mol Cell Biol 30, 897–907.

Isnard AD, Thomas D, Surdin-Kerjan Y (1996). The study of methionine uptake in Saccharomyces cerevisiae reveals a new family of amino acid permeases. J Mol Biol 262, 473–484.

Jensen LT, Carroll MC, Hall MD, Harvey CJ, Beese SE, Culotta VC (2009). Down-regulation of a manganese transporter in the face of metal toxicity. Mol Biol Cell 20, 2810–2819.

Jones E, Oliphant E, Peterson P, et al. (2001). SciPy: open source scientific tools for Python. Available at www.scipy.org (accessed 2 August 2016).

Kang Y, Zhou XE, Gao X, He Y, Liu W, Ishchenko A, Barty A, White TA, Yefanov O, Han GW, et al. (2015). Crystal structure of rhodopsin bound to arrestin by femtosecond X-ray laser. Nature 523, 561–567.

Katzmann DJ, Babst M, Emr SD (2001). Ubiquitin-dependent sorting into the multivesicular body pathway requires the function of a conserved endosomal protein sorting complex, ESCRT-I. Cell 106, 145–155.

Keener JM, Babst M (2013). Quality control and substrate-dependent downregulation of the nutrient transporter Fur4. Traffic 14, 412–427.

Kirchhofer A, Helma J, Schmidthals K, Frauer C, Cui S, Karcher A, Pellis M, Muyldermans S, Casas-Delucchi CS, Cardoso MC, et al. (2010). Modulation of protein properties in living cells using nanobodies. Nat Struct Mol Biol 17, 133–138.

Kommaddi RP, Shenoy SK (2013). Arrestins and protein ubiquitination. Prog Mol Biol Transl Sci 118, 175–204.

Kulak NA, Pichler G, Paron I, Nagaraj N, Mann M (2014). Minimal, encapsulated proteomic-sample processing applied to copy-number estimation in eukaryotic cells. Nat Methods 11, 319–324.

Li M, Rong Y, Chuang YS, Peng D, Emr SD (2015). Ubiquitin-dependent lysosomal membrane protein sorting and degradation. Mol Cell 57, 467–478.

Li SC, Kane PM (2009). The yeast lysosome-like vacuole: endpoint and crossroads. Biochim Biophys Acta 1793, 650–663.

Lin CH, MacGurn JA, Chu T, Stefan CJ, Emr SD (2008). Arrestin-related ubiquitin-ligase adaptors regulate endocytosis and protein turnover at the cell surface. Cell 135, 714–725.

MacGurn JA, Hsu PC, Emr SD (2012). Ubiquitin and membrane protein turnover: from cradle to grave. Annu Rev Biochem 81, 231–259.

MacGurn JA, Hsu PC, Smolka MB, Emr SD (2011). TORC1 regulates endocytosis via Npr1-mediated phosphoinhibition of a ubiquitin ligase adaptor. Cell 147, 1104–1117.

Mattiroli F, Sixma TK (2014). Lysine-targeting specificity in ubiquitin and ubiquitin-like modification pathways. Nat Struct Mol Biol 21, 308–316.

Menant A, Barbey R, Thomas D (2006). Substrate-mediated remodeling of methionine transport by multiple ubiquitin-dependent mechanisms in yeast cells. EMBO J 25, 4436–4447.

Merhi A, Andre B (2012). Internal amino acids promote Gap1 permease ubiquitylation via TORC1/Npr1/14-3-3-dependent control of the Bul arrestin-like adaptors. Mol Cell Biol 32, 4510–4522.

Nabhan JF, Pan H, Lu Q (2010). Arrestin domain-containing protein 3 recruits the NEDD4 E3 ligase to mediate ubiquitination of the beta2-adrenergic receptor. EMBO Rep 11, 605–611.

Nikko E, Pelham HR (2009). Arrestin-mediated endocytosis of yeast plasma membrane transporters. Traffic 10, 1856–1867.

Novoselova TV, Zahira K, Rose RS, Sullivan JA (2012). Bul proteins, a non-redundant, antagonistic family of ubiquitin ligase regulatory proteins. Eukaryot Cell 11, 463–470.

O'Donnell AF, Apffel A, Gardner RG, Cyert MS (2010). Alpha-arrestins Aly1 and Aly2 regulate intracellular trafficking in response to nutrient signaling. Mol Biol Cell 21, 3552–3566.

Patwari P, Emilsson V, Schadt EE, Chutkow WA, Lee S, Marsili A, Zhang Y, Dobrin R, Cohen DE, Larsen PR, et al. (2011). The arrestin domain-containing 3 protein regulates body mass and energy expenditure. Cell Metab 14, 671–683.

Piper RC, Dikic I, Lukacs GL (2014). Ubiquitin-dependent sorting in endocytosis. Cold Spring Harb Perspect Biol 6, a016808.

Polekhina G, Ascher DB, Kok SF, Beckham S, Wilce M, Waltham M (2013). Structure of the N-terminal domain of human thioredoxin-interacting protein. Acta Crystallogr D Biol Crystallogr 69, 333–344.

Prosser DC, Pannunzio AE, Brodsky JL, Thorner J, Wendland B, O'Donnell AF (2015). a-Arrestins partipate in cargo selection for both clathrin-independent and clathrin-mediated endocytosis. J Cell Sci 128, 4220–4234.

Qi S, O'Hayre M, Gutkind JS, Hurley JH (2014). Insights into beta2-adrenergic receptor binding from structures of the N-terminal lobe of ARRDC3. Protein Sci 23, 1708–1716.

Rotin D, Staub O, Haguenauer-Tsapis R (2000). Ubiquitination and endocytosis of plasma membrane proteins: role of Nedd4/Rsp5p family of ubiquitin-protein ligases. J Membr Biol 176, 1–17.

Santiago M, Gardner RC (2015). Yeast genes required for conversion of grape precursors to varietal thiols in wine. FEMS Yeast Res 15, fov034.

Shaner NC, Lin MZ, McKeown MR, Steinbach PA, Hazelwood KL, Davidson MW, Tsien RY (2008). Improving the photostability of bright monomeric orange and red fluorescent proteins. Nat Methods 5, 545–551.

Shea FF, Rowell JL, Li Y, Chang TH, Alvarez CE (2012). Mammalian alpha arrestins link activated seven transmembrane receptors to Nedd4 family e3 ubiquitin ligases and interact with beta arrestins. PLoS One 7, e50557.

Shi Y, Stefan CJ, Rue SM, Teis D, Emr SD (2011). Two novel WD40 domain-containing proteins, Ere1 and Ere2, function in the retromer-mediated endosomal recycling pathway. Mol Biol Cell 22, 4093–4107.

Shukla AK, Manglik A, Kruse AC, Xiao K, Reis RI, Tseng WC, Staus DP, Hilger D, Uysal S, Huang LY, et al. (2013). Structure of active beta-arrestin-1 bound to a G-protein-coupled receptor phosphopeptide. Nature 497, 137–141.

Shukla AK, Westfield GH, Xiao K, Reis RI, Huang LY, Tripathi-Shukla P, Qian J, Li S, Blanc A, Oleskie AN, et al. (2014). Visualization of arrestin recruitment by a G-protein-coupled receptor. Nature 512, 218–222.

van der Walt S, Schonberger JL, Nunez-Iglesias J, Boulogne F, Warner JD, Yager N, Gouillart E, Yu T, scikit-image C (2014). scikit-image: image processing in Python. PeerJ 2, e453.

Weinberg J, Drubin DG (2012). Clathrin-mediated endocytosis in budding yeast. Trends Cell Biol 22, 1–13.

Zhao Y, Macgurn JA, Liu M, Emr S (2013). The ART-Rsp5 ubiquitin ligase network comprises a plasma membrane quality control system that protects yeast cells from proteotoxic stress. Elife 2, e00459.